Int J Adv Manuf Technol (2016) 87:2567–2579
DOI 10.1007/s00170-016-8614-4

ORIGINAL ARTICLE

Characterization of microstructure, chemical composition, and toughness of a multipass welded joint of austenitic stainless steel AISI316L

Mustafa Tümer[1] · **Ramazan Yılmaz**[2]

Received: 24 March 2015 / Accepted: 7 March 2016 / Published online: 31 March 2016

Abstract In this study, AISI 316 types of austenitic stainless steels were welded by FCAW (flux-cored arc welding) using E316LT1-1/4 flux-cored wire under various shielding gas mixtures containing CO_2 at different ratios. Effects of mixed ratio of Ar and CO_2 in the in the shielding gas on the microstructure, impact toughness, and microhardness of welded materials were studied. Stereo optical microscopy, scanning electron microscopy (SEM), energy dispersive spectroscopy (EDS), transmission electron microscope (TEM), and TEM/mapping analysis techniques were used for microstructural characterizations. The impact toughness values of the weldments were decreased as a result of the formation and growth of inclusions in the microstructure due to the increases amount of CO_2 in the shielding gas. The hardness values and δ-ferrite amount in the weld metal were affected by depending on of the shielding gas mixtures.

Keywords Flux cored arc welding · Stainless steel · δ-ferrite · Shielding gas · Inclusion

✉ Mustafa Tümer
mustafa.tumer@kocaeli.edu.tr

Ramazan Yılmaz
ryilmaz@sakarya.edu.tr

[1] Department of Welding Technology, Uzunçiftlik Nuh Çimento Vocational High School, Kocaeli University, Kocaeli, Türkiye

[2] Department of Metallurgical and Materials Engineering, Technology Faculty, Sakarya University, Esentepe, Sakarya, Türkiye

1 Introduction

AISI 316 L austenitic stainless steel materials have a wide range of usage area for their superior mechanical and corrosion properties. They are commonly preferred in energy industries such as ship building, chemistry, defense, nuclear energy, and cryogenic applications. Compared to other stainless steels, austenitic stainless steel is distinguished with its excellent corrosion resistance and high toughness characteristics. Due to the internal structure being austenitic, embrittlement, which is a significant problem encountered in ferritic stainless steels and seen under transition temperature, is not observed in this type of steels. Furthermore, their resistance to intergranular corrosion is high due to low carbon content. Their toughness properties are significantly good, and no martensite transformation is observed during cooling. Therefore, cold cracking problems are not observed in joining austenitic stainless steels as in ferritic martensitic stainless steels, and no pre-heating during joining and post-welding heat treatment are required [1–5].

Flux-cored arc welding (FCAW) method is used in joining thick section stainless steels in today's industry, which leads to a considerable increase in production speed of welding treatments. Welding performed by using flux-cored arc is a more economical and efficient method compared to other welding methods due to its high melting power, suitability for automation for continuous welding process, its usability in every position, ease of performance, and smooth weld nuggets with high mechanical properties. Slag formation in welding and protection of weld metal by shielding gas ensure less oxidation of nugget surfaces in welds performed with flux cored wires and minimization of foreign matters in weld bath [5–9].

Table 1 Chemical compositions of base and filler material used

Elements	C	Si	Mn	Cr	Ni	Mo
AISI 316L	0.016	0.801	1.609	16.44	9.590	1.719
E316LT1-1/4	0.028	0.60	1.50	18.35	12.65	2.68

In order to ensure the safety of constructions formed with welded joints, mechanical and microstructural characterization of the weld metal obtained as a result of the joining must be performed elaborately. Quality of joint varies depending on parameters such as metal transfer rate, heat input, welding seam geometry, and the shielding gas composition used. Being one of the most significant parameters during the welding treatment, shielding gas protects weld metal from the adverse effects of the nitrogen and oxygen contained in the atmosphere and ensures steady arc and uniform metal transfer. Therefore, type and composition of the gas used considerably affect the microstructure and mechanical characteristics of the joined material [10–18].

FCAW method used in joining thick section stainless steels has gradually become widespread in recent years. Superiorities of the FCAW method over the other welding methods and usability of active shielding gas increase the prefer ability of the method. Additional stainless steel flux-cored wires are designed so as to be used with Ar-CO_2 or 100 % CO_2 shielding gasses. High arc energy given by CO_2 gas provides a higher melting speed and satisfactory penetration based on other shielding gas types. Moreover, its oxidative effect in welding arc plasma results in oxidation of the elements contained in the stainless steel such as Mn, Si, Al, Cr, and Ti [11–14, 16]. Some studies have reported that this situation was reported to have a higher amount of inclusion content compared to the alkaline-based additional weld metals due to the fact that it causes inclusion formation in weld metal and the rutile-based additional weld metals have low purification capability [16, 19].

In literature; Cleiton et al., [20] joined AISI 316 L austenitic stainless steel material with E309MoL-16 additional weld metal at different heat inputs. It was reported in the feritscope measurements performed after the joining process that increasing of heat input caused a reduction in δ-ferrit amounts. Arivazhagan et al. [16] joined modified 9Cr-1Mo material by using the FCAW method and examined the effect of shielding gas, mixed of Ar and CO_2, on mechanical properties, and they determined that as the CO_2 amount contained in the mixture rate increased, the amount of oxygen contained in dissolved weld metal increased and also the mechanical values decreased and the inclusion amount contained in weld metal increased. It has been shown in numerous studies that it affects composition of the shielding gas used in welding treatment and microstructure and consequently mechanical properties of materials joined as multipass [8, 12–16, 21]. However, characterization of the microstructural transformations occurred and the inclusions in oxide form and also their effect on mechanical values were not studied in detail. What makes this study differ from others is that AISI 316 L material joined by using the FCAW method at four shielding gas compositions (Ar-12 % CO_2, Ar-20 % CO_2, Ar-50 % CO_2, and 100 % CO_2) was examined by performing notch impact tests and microstructure studies and characterizing the δ-ferrit amount and the inclusions in weld metal with appropriate methods.

2 Experimental procedure

The chemical composition of the AISI 316 L austenitic stainless steel material and E316LT1-1/4, rutile type flux cored wire, used in this study is given in Table 1. Multipass welding processes were carried out with a semi-automatic oscillating device, in order to see the effect of shielding gasses during the welding process (Fig. 1a). The interpass temperature was kept under constant control (<150 °C) to prevent faults that may occur due to overheating. Depending on the welding parameters, the heat input kept under control between 0.9 and 1.4 $kJmm^{-1}$ for all passes. In addition to that short circuiting transfer mode in first pass and spray transfer mode with small

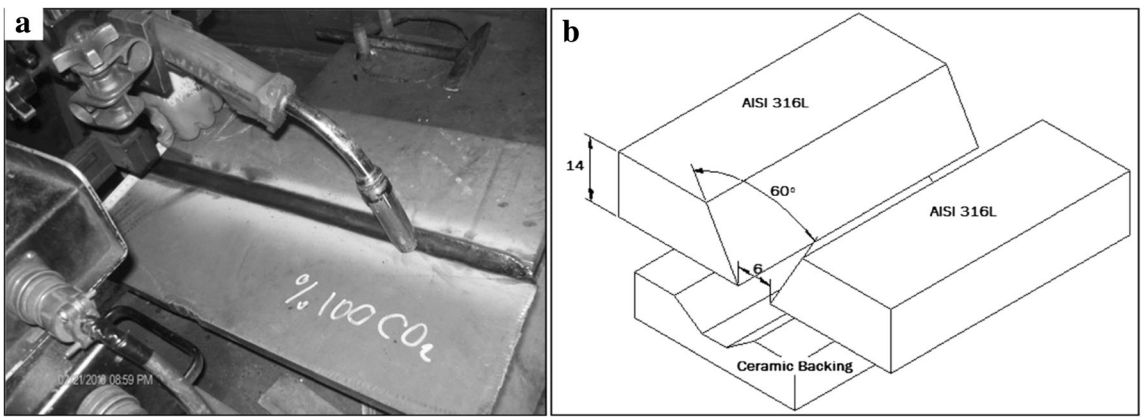

Fig 1 **a** The assembly of welding equipments and performing of the welding. **b** Scheme of joint preparation

Table 2 Welding conditions and parameters used

Passes	Current (A)	Voltage (V)	Welding speed (mms^{-1})	Heat input ($kJmm^{-1}$)
1	180	30	4.83	1.1
2	250	35	5.38	1.6
3	260	35	5.17	1.8
4	212	32	4.82	1.4
5	212	32	4.82	1.4
6	220	33	5.33	1.3

amount of spatter in the other passes were occurred during the welding process. As understood from earlier literature [22, 23], metal transfer mode during FCAW process depends on welding parameters such as current and voltage values, electrode size, composition of electrode, and shielding gasses. In order to achieve a spray transfer, higher current and larger diameter electrode are needed. A shielding gas of carbon dioxide (CO_2) and mixture of CO_2 and argon also provide spray transfer. Therefore, shielding gas composition one of the most important parameters and contributes to spray transfer mode during welding process. Plates ($450 \times 150 \times 14$ mm^3) were used for producing the joints and a 60° single V groove edge preparation was followed with a root face/gap of 6 mm as shown in Fig. 1b. Ceramic backing was used in the joints. Four different gasses were used as shielding gas, which were Ar-12 % CO_2, Ar-20 % CO_2, Ar-50 % CO_2, and 100 % CO_2. The shielding gas flow rate was applied as 15 l/min. Table 2 shows the parameters used in welding.

Charpy impact test specimens were obtained from the weld metal samples, and the experiments were carried out using the test temperatures of −40 °C, −20 °C, 0 °C, and 20 °C as the reference temperatures. Three Charpy impact tests were conducted for each temperature, and the arithmetic average was taken. Various sizes of welding samples removed from the welded pieces were subjected to metallographic processes for microstructural analysis. Samples readied for microstructure analysis were electrolytically etched in 10 % of oxalic acid solution, at 10.4 V for 15 s. After etching, NIKON SMZ800 stereo microscope was used first to examine the macrostructure, and NIKON ECLIPSE L150 optical microscope was used to examine the microstructure of the pieces. The chemical composition analysis in percentage weight of the cross-sectional samples extracted from the welded materials was performed with the Foundry Master Pro brand Optical Emission Spectrometer. Chemical analysis was performed on 3 regions of the weld metal, and the measurement results were averaged. The microhardness process was carried out by applying an image-controlled 200-g load with Struers DuraScan 20 brand device. Ferrite content measurements of the welds in ferrite percentage were performed with a Fischer Ferritscope across the weld zones. X-ray diffractometer (XRD) analyses were performed on the samples that present the highest and lowest mechanical values in order to determine δ-ferrite and austenite phase amounts. XRD analyses were carried out in GBC MMA 027 brand X-ray device, at 28.8 mA, 25 kV power values by using CuKα tube, with 0.2° of scanning increments in the range of 2θ/40–120°. The image of the inclusions occurred in the weld metal was taken with

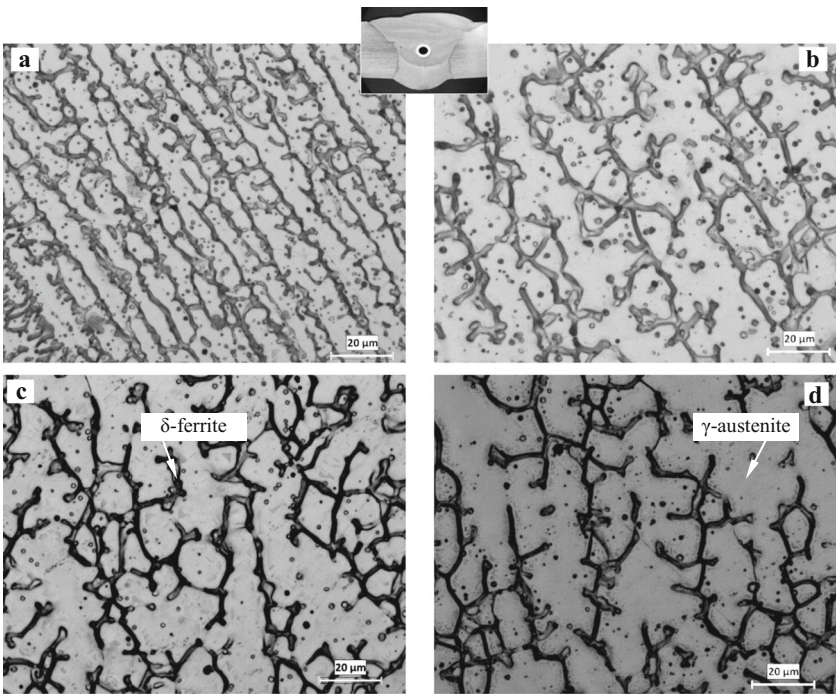

Fig. 2 Weld metal microstructure **a** Ar-%12 CO_2 **b** Ar-%20 CO_2 **c** Ar-%50 **d** %100 CO_2

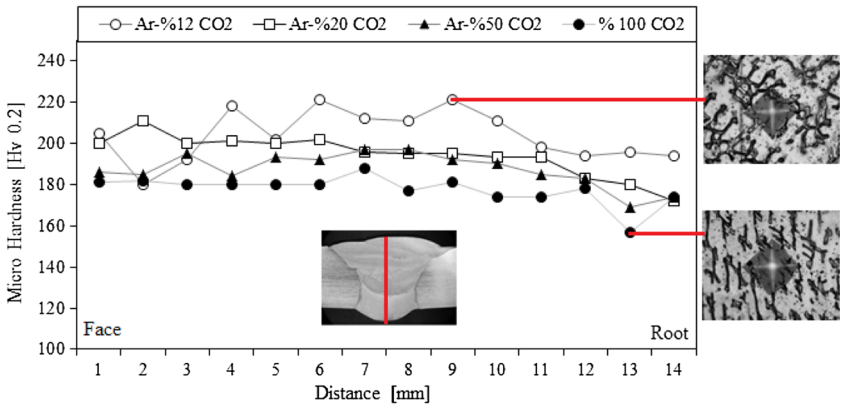

Fig. 3 Vickers microhardness values

JEOL JSM-6060LV brand scanning electron microscopy (SEM), and its characterization was obtained with JEOL HRTEM brand transmission electron microscopy (TEM) and with energy-dispersive spectrometry (EDS). For TEM analysis, samples were formed into a thin foil (200 μm), and after thinning mechanically, they were electrolytically etched at −30 °C in 80 % alcohol—20 % perchloric acid solution.

3 Results and discussion

3.1 Microstructure

The microstructure images taken from the weld metal of the AISI 316 L austenitic stainless steel material welded with the FCAW method by using different shielding gas are shown in Fig. 2. In the images, dark-colored areas indicate δ-ferrite, and the light-colored regions indicate the austenite phase. The amount of CO_2 in the shielding gas affects the δ-ferrite ratio formed in the microstructure. Low amount of CO_2 (Ar-12 % CO_2) in shielding gas cases decreased heat input and caused rapid cooling of weld metal during the welding process, which provided to increase in δ-ferrite amount in weld metal. δ-ferrite content formed in the microstructure decreases with the increase in the amount of CO_2 in the shielding gas, and this causes the expansion of the austenite area. Moreover, morphology of the δ-ferrite that forms depending on the composition of the shielding gas also varies. When performing welding in low amounts of CO_2 shielding gas, the dendritic branches of δ-ferrite form in linear elongation shape, whereas with the increase in the amount of CO_2, breaks, openings, and splits were observed in dendrite branches with the welding performed in especially the Ar-50 % CO_2 and 100 % CO_2. Since the weld is the same kind of metal, the effect of melting occurred in the main material on the microstructure is negligible. The cooling rate is higher in the first pass, due to the multi-pass nature of the welding. However, the weld metal is exposed to more thermal cycles with the later welding passes. The δ-ferrite phase that forms spherical chains rather than dendrite branches has caused splits of the bonds between the branches with the increased amount of CO_2 in the shielding gas. This is supported by the similar previous studies [12]. The increase in the amount of CO_2 in the shielding gas leads to an increase in arc voltage of the ionization, disassociation, and recombination energies created during the welding process and affects the seam form, the drop transition mechanism, and arc energy during welding [24–27]. As a result of this situation, the heat input increases, and weld pool reaches to a higher temperature. Thus, the cooling rate of the weld metal slows down, and remaining at the critical transformation temperature for longer periods causes the expansion of the austenite area in microstructures of the weld metal. It has been reported in previous studies that the morphology of the δ-ferrite in the weld metal varies depending on the temperature and cooling rate [10–14, 28]. Comparing the base material with the weld metal, rapid cooling in the weld metal causes lesser amounts austenite formation [12, 29].

Table 3 Results of chemical analysis conducted on weld metal of AISI 316 L material

Elements	Ar-% 12 CO_2	Ar-% 20 CO_2	Ar-% 50 CO_2	CO_2
C	0.0225	0.0207	0.0201	0.0191
Si	0.707	0.615	0.57	0.505
Mn	1.65	1.37	1.37	1.26
Cr	18.13	18.14	18.12	17.89
Mo	3.09	2.82	2.83	2.74
Ni	12.65	12.83	12.87	12.73
Cu	0.084	0.0952	0.0949	0.0965
Nb	0.019	0.0199	0.0186	0.0171
Ti	0.0549	0.0739	0.0742	0.0573

3.2 Microhardness measurements

Figure 3 shows the microhardness measurements have been carried out from the weld surface to the root pass in a straight line. In the microhardness measurements taken from the center of the weld metal longitudinally, the

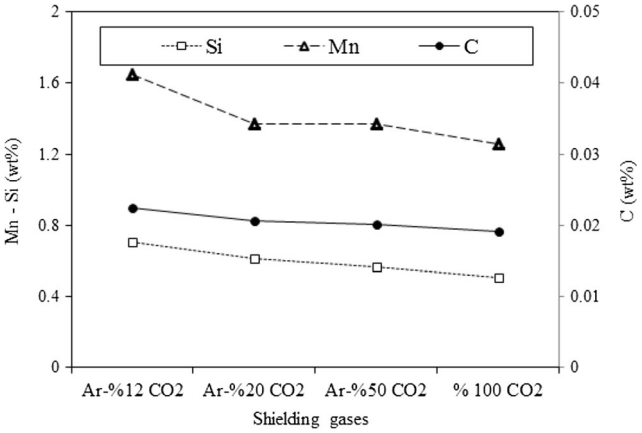

Fig. 4 Variation C, Mn, and Si element contents in the weld metal according to shielding gas

highest hardness value was obtained as 221 $HV_{0.2}$ in the weld metal welded with the Ar-12 % CO_2 shielding gas in general. And the lowest hardness value was measured as 157 $HV_{0.2}$ in the weld metal welded with CO_2 shielding gas. Microhardness values increase depending on the increasing amount of δ-ferrite in the weld metal. Since the hardness values taken from various points of the weld metal vary depending on the amount of δ-ferrite at the point of hardness, the hardness values taken at the same region can vary. The higher microhardness values in the material welded with Ar-12 % CO_2 shielding gas are to be expected because of the δ-ferrite content. The results obtained in this study are in line with an earlier study [8, 11, 12, 20].

3.3 Chemical analysis

The chemical analysis results of the weld metal of the AISI 316 L material welded with the E316LT-1/4 flux core wire are given in Table 3. Analyzing the results of the spectrometer, the variation of the C, Mn, and Si elements in the weld metal is noteworthy depending on content of shielding gas. The C content of the sample that was welded with the shielding gas containing Ar-12 % CO_2 was 0.0225 %, whereas C content of the sample welded with a 100 % CO_2 was 0.0191 %. An increase in the amount of CO_2 in the shielding gas has been

Table 4 Ferrite content analysis of the welded joints (δ-ferrite %)

Measurement areas	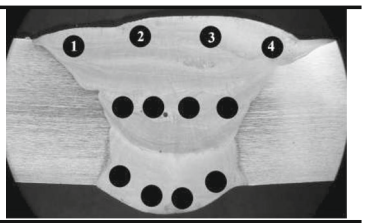			
	Ar - %12 CO_2			
	1.	**2.**	**3.**	**4.**
Face	12,9	18,2	17,5	11,2
Middle	13	14,8	15	12
Root	12,1	14,6	13,2	11,5
	Ar - %20 CO_2			
	1.	**2.**	**3.**	**4.**
Face	9,2	12,7	12,9	10,2
Middle	9,3	11,3	12,2	9,2
Root	9,8	9,4	10,1	9,8
	Ar - %50 CO_2			
	1.	**2.**	**3.**	**4.**
Face	9,8	11,8	12	8,2
Middle	8,3	9,2	9,8	6,6
Root	8,1	8,3	8,5	8
	%100 CO_2			
	1.	**2.**	**3.**	**4.**
Face	9,4	9,9	10,4	9,6
Middle	7,7	8,8	9,3	8,4
Root	7,6	8	7,3	6,9

found to cause a decrease in the Si, Mn elements in the weld metal. The amounts of Si and Mn in the weld metal welded with Ar-12 % CO_2 shielding gas were 0.707 and 1.65 %; whereas the amounts of Si and Mn in the weld metal welded with 100 % CO_2 shielding gas were 0.505 and 1.26 %, respectively (Fig. 4). The presence of O_2 and CO_2 gasses in the shielding gas composition causes the loss of the main alloying elements such as Mn and Si during the passage of the molten droplet in the arc. However, as the amount of CO_2 in the shielding gas increases the formation of oxides such as MnO and SiO_2 also increases, and a large amount of them are moving away from the weld metal as a slag, a certain amount of them remains in the weld metal as inclusions [12, 13, 16].

3.4 Ferrite measurements

The variation of the amount of δ-ferrite in the weld metal obtained by welding the AISI 316 L austenitic stainless steel with different shielding gasses with the FCAW method is given in Table 4. The highest δ-ferrite ratio of 13.8 % was obtained in the weld metal welded with the Ar-12 % CO_2 shielding gas, according the averaged measurements taken from the root, middle, and surface parts of the weld metal. And the lowest δ-ferrite ratio of 8.6 % was measured in the weld metal welded with the 100 % CO_2 shielding gas. It was seen that the amount of δ-ferrite increased in the central part of the weld metal and decreased in the vicinity of the base material. This was thought to be caused by melting and the cooling rate occurred in the austenitic base material. It was observed that the measurement results taken from the middle and lower part of the weld metal were lower than the measurement results in the upper area, and similar results were obtained along the line, especially on the lower sections. The δ-ferrite ratio in the weld metal welded with Ar-12 % CO_2 shielding gas was found to be higher regionally in all

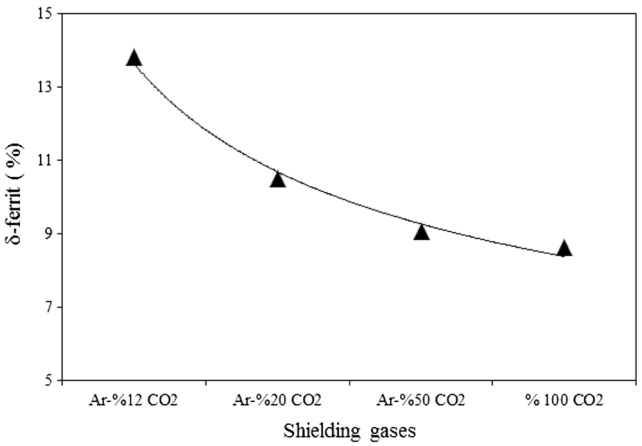

Fig. 5 Measurements of δ-ferrite content (%)

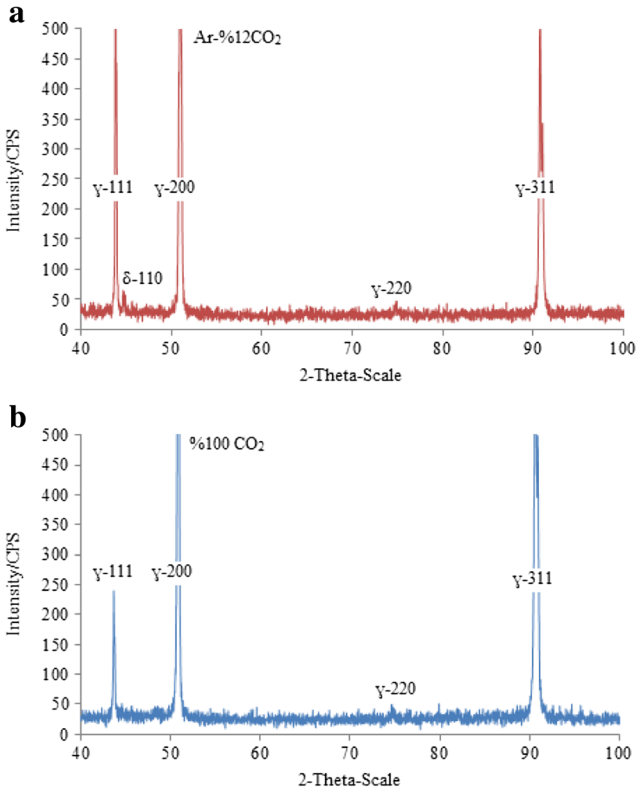

Fig. 6 X-Ray diffraction analyze of weld metal **a** Ar-%12 CO_2 **b** %100 CO_2

measurements taken from the root, intermediate, and cover passes of the weld metal. According to the results obtained, the lower amount of δ-ferrite obtained in the CO_2 shielding gas supports the microstructure results. The amount of δ-ferrite increases because of the faster solidification in the cover pass. Figure 5 shows the average percentage of δ-ferrite amount obtained by the measurement performed via feritscope graphically.

It is observed in the general measurement values that the amount of δ-ferrite on the cover passes of the weld metal is excessive. The reason for this is the faster solidification on the cover passes and as a result the insufficient time for austenite transformation due to sample's shorter exposure to transition temperature. Also, since the middle and lower passes were exposed to the thermal cycle in the next pass, they remained in the transition temperature longer than the cover pass. Thus, much more austenite transformation was occurred.

Table 5 Impact energy values of welds

Shielding gasses	Test temperature (°C)	20	0	−20	−40
Ar-%12 CO_2	Impact energy values (J)	84	77	75	67
Ar-%20 CO_2		81	77	69	63
Ar-%50 CO_2		68	68	63	59
%100 CO_2		65	65	56	50

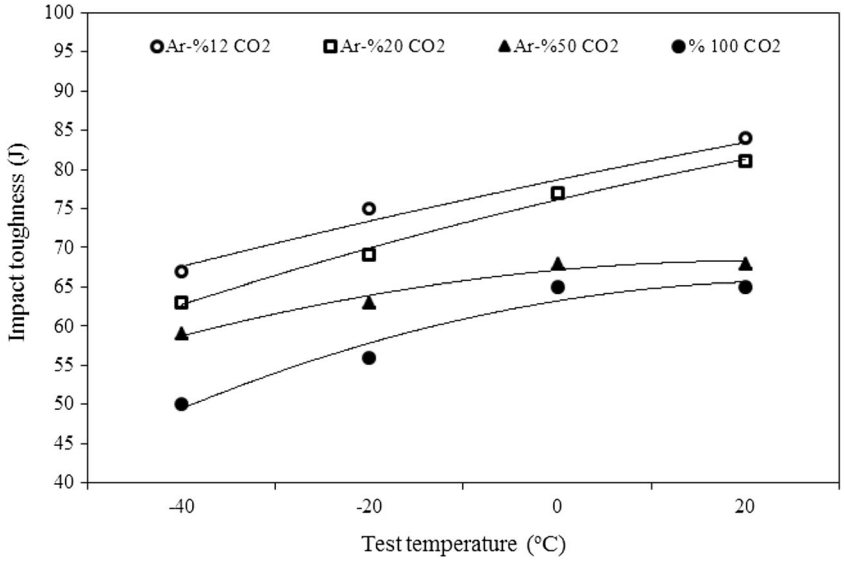

Fig. 7 Variation of the notch impact toughness values as a function of the shielding gas and test temperature

3.5 XRD analyze

XRD analysis is applied for the phase analysis in the weld metal (Fig. 6). It was observed in the weld metals of the samples welded with Ar-12 % CO_2 and 100 % CO_2 shielding gasses that all peaks were created in the austenite phase. Feritscope measurements revealed that 13.8 % δ-ferrite was present in the weld metal of the weldment with Ar-12%CO_2 shielding gas. In the XRD analysis applied to the weld metal of the sample welded with Ar-12 % CO_2 shielding gas, 2θ-45, 5° low intensity δ-ferrite (1 1 0) peak was identified. All other diffraction patterns represent γ-austenite phase. γ (2 0 0) and γ (3 1 1) γ diffraction peaks contained in weld metal show the highest and greater quantities of phases. In contrast, γ (1 1 1) and γ (2 2 0) diffraction peaks are the lowest and the least amount of phases in all of the weld metal. And this shows that the interior structure is formed by austenite and small amount of δ-ferrite phase in general. No δ-ferrite peaks were observed in the sample welded with 100 % CO_2 shielding gas. Results are compatible with feritscope measurements and the microstructural images given in the previous sections. Moreover, the results are also consistent with XRD analysis results taken

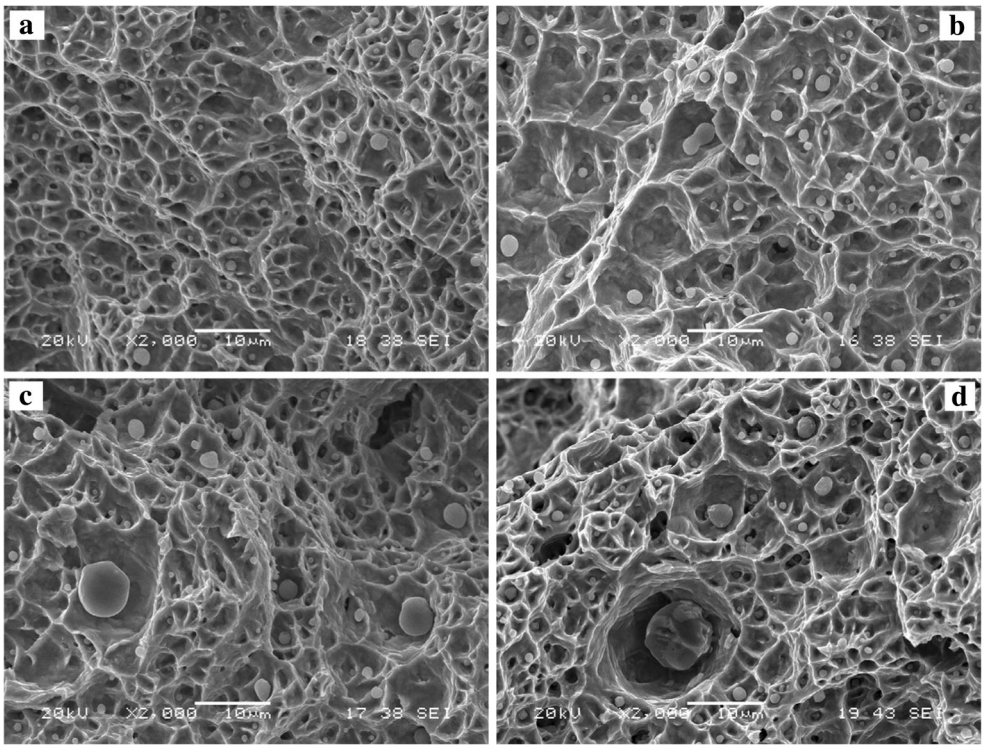

Fig. 8 SEM fractographs of fractured Charpy impact samples welded under shielding gas of (20 °C) **a** %12 CO_2 **b** %20 CO_2 **c** %50 CO_2 **d** %100 CO_2

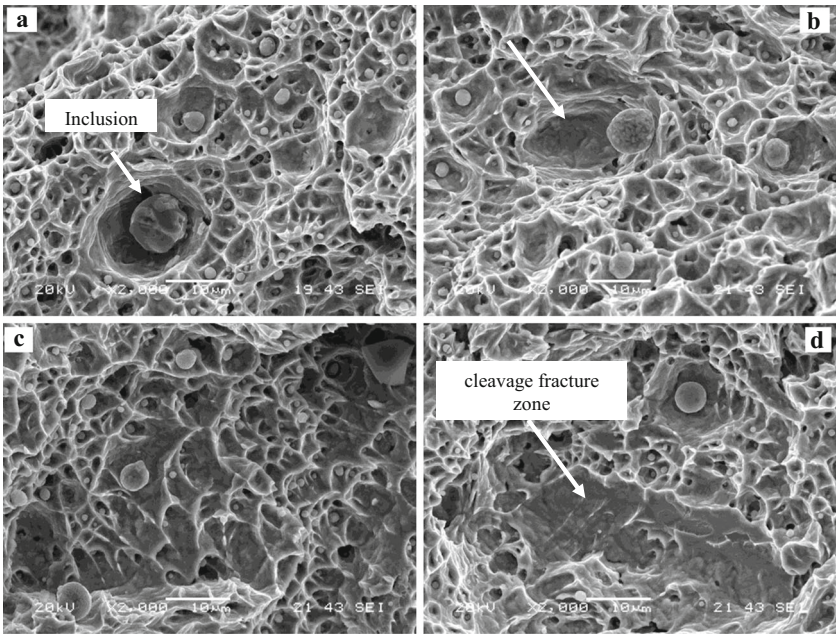

Fig. 9 SEM fractographs of Charpy impact test samples welded under %100 CO_2 fractured at temperatures of **a** 20 °C **b** 0 °C **c** −20 °C **d** −40 °C

from the welding of similar materials [18, 30]. Very small quantities (8.6 %) of δ-ferrite phase are present in the weld metal of the material welded with 100 % CO_2 gas. Therefore, this amount is not present in the XRD graphs. In addition, the carbide precipitation, Cr_2N, or intermetallic phases were also not found in X-ray diffraction analysis. This is advantageous for both the mechanical properties and the corrosion resistance of the weld metal [30].

3.6 Impact toughness and fracture surface

The impact strength values that vary depending on the type of shielding gas used during the welding process are given in Table 5 and shown in Fig. 7 graphically. Looking at the Table and Figure, the Charpy impact test, test temperature, and the amount of CO_2 in the shielding gas composition affect the fracture energy values. A decrease in Charpy impact toughness values is observed as the amount of CO_2 in the shielding gas increases. In addition, Charpy impact test temperature also affects the fracture toughness energies, and lower toughness values are obtained at low temperatures. In general, comparing the resulting fracture energies, impact toughness of the sample welded with Ar-12 % CO_2 shielding gas varies between 84 and 67 J, depending on the test temperature. This value range was obtained as 81-65 J with Ar-20 % CO_2, 68-59 J with Ar-50 % CO_2 and 65-50 J with 100 % CO_2. In the Charpy impact tests, the highest impact toughness energy value at room temperature occurred at 84 J in the welding performed with Ar-12 CO_2 gas. And the lowest impact toughness value was 50 J in the Charpy impact test performed at −40 °C in the weld metal welded with 100 % CO_2 gas.

The structure of the austenitic phase is advantageous for achieving high toughness in tests conducted at lower temperatures. The amount of δ-ferrite content decreases depending on the amount of CO_2 in the shielding gas composition. This can be considered to cause a slight decrease in impact toughness depending on the temperature. Therefore, there is a slight decrease in the samples with an increase in the austenite phase, despite the expected increase in the toughness values. During the welding process carried out by the method of FCAW, the inclusions formed in the microstructure in parallel with the increase in CO_2 shielding gas cause lower toughness strength in the samples with higher austenite percentage.

SEM images of fracture surfaces after impact test are shown in Fig. 8. Looking at the fracture surfaces resulted in the experiments conducted at different temperatures on weld metals with different shielding gasses, typical ductile fracture morphology of austenitic stainless steels is observed. The

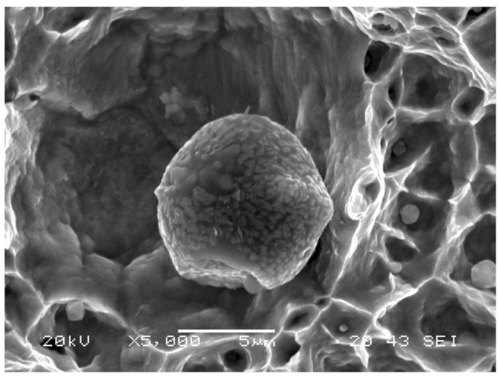

Fig. 10 SEM image of inclusion

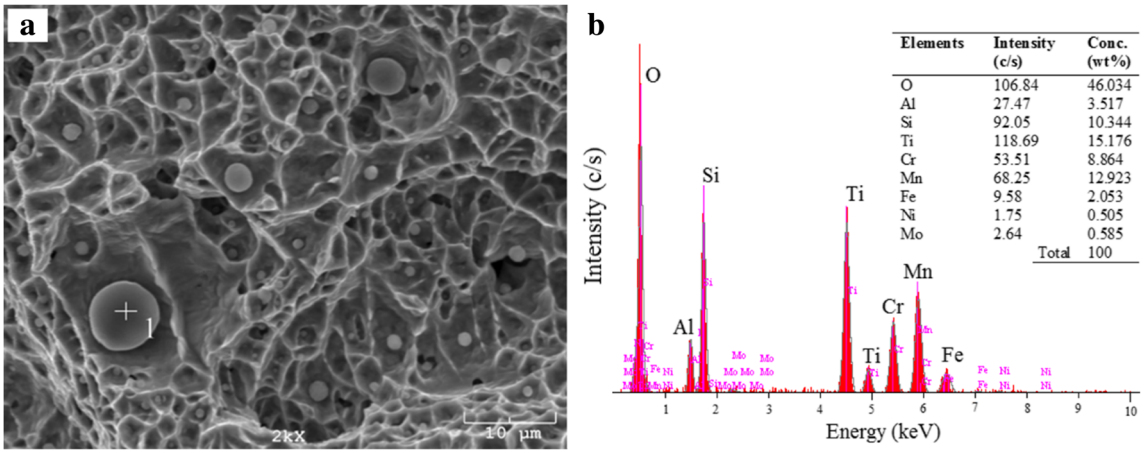

Fig. 11 Fracture surface of charpy impact sample welded under pure CO_2 and EDS analysis results of inclusion

inclusions are created in dimples that form the network structure. Inclusions have spherical forms. The size of the inclusions and the size of the created pits increase as the amount of CO_2 in the shielding gas increases. During the welding process, an increase in the amount of CO_2 in the shielding gas creates various reactions. It can dissociate in the arc to release oxygen and carbon monoxide and this can result in a reduction in the weld metal content of elements such as silicon, manganese and titanium. This case leads to increase in number and size of inclusions in the weld metal [26]. A decrease in terms of size and distribution of the inclusions was observed in the weld metal obtained with shielding gas containing higher amounts of Argon. Additionally, it was observed that the inclusions expand the dimensions of the pits that they are located in. Expanding pits affect the Charpy impact results and cause the decrease of the toughness values in line with the increase in CO_2 gas in the shielding gas.

Fracture surface images obtained after Charpy impact test carried at different temperatures of the material welded with only the 100 % CO_2 gas are shown in Fig. 9. Partial cleavage fracture zones on the surface of fracture has occurred when the test temperature decreased to −40 °C, in the fracture surfaces of the material welded at lower impact temperatures with 100 % CO_2 shielding gas. Inclusions present in the microstructure during the impact test are believed to accelerate the formation and propagation of the fractures during the dynamic test. Thus, it leads to decrease in the amount of energy used for formation and propagation of the fracture during the Charpy impact test. The lower impact toughness values obtained and the inclusions found in the earlier studies on the fracture surfaces after the Charpy impact test of the austenitic stainless steel material are in line with the results obtained in this study [8, 11–14, 16, 17].

According to the microstructure images and feritscope measurements given in the previous sections, it is seen that impact toughness values of the samples with higher δ-ferrite content in the weld metal are also higher at all temperatures. As it is known, δ-ferrite has body-centered cubic (BCC) structure and accordingly the values obtained in the Charpy impact tests vary depending on the temperature. Lower values are obtained at lower test temperatures [31]. And impact toughness value of austenitic phase having face-centered cubic (FCC) structure is independent of temperature provides advantages to materials joined even at low temperatures.

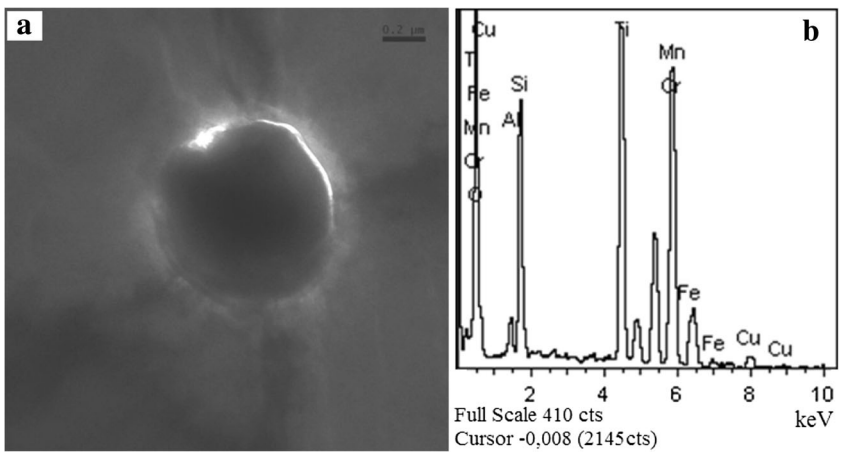

Fig. 12 **a** TEM images and **b** EDS analyze of the weld metals performed under %100 CO_2 shielding gas

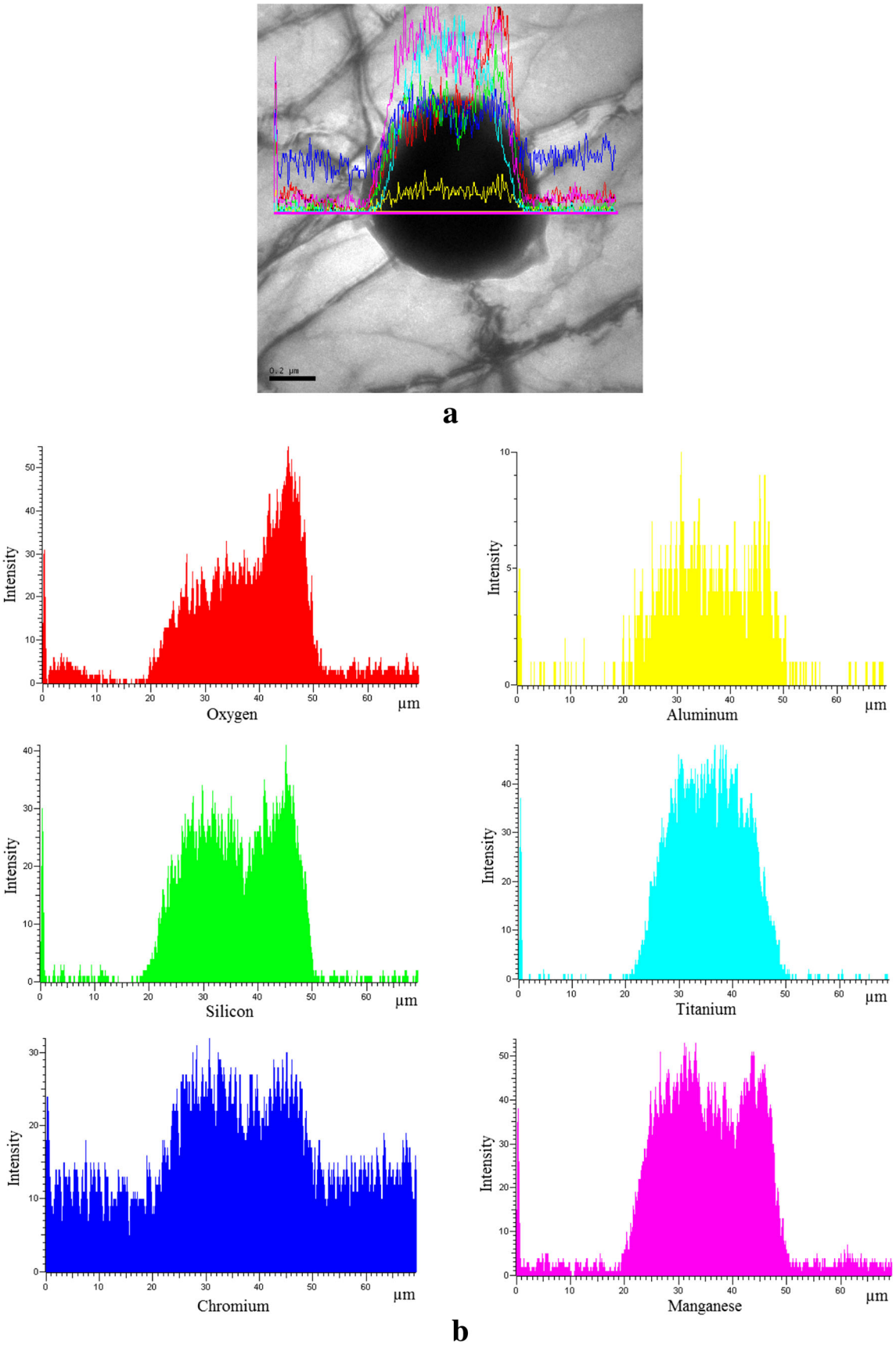

Fig. 13 **a** TEM-EDS line scan showing variation alloying elements across the weld metal **b** EDS analysis of linear graphs of the elements

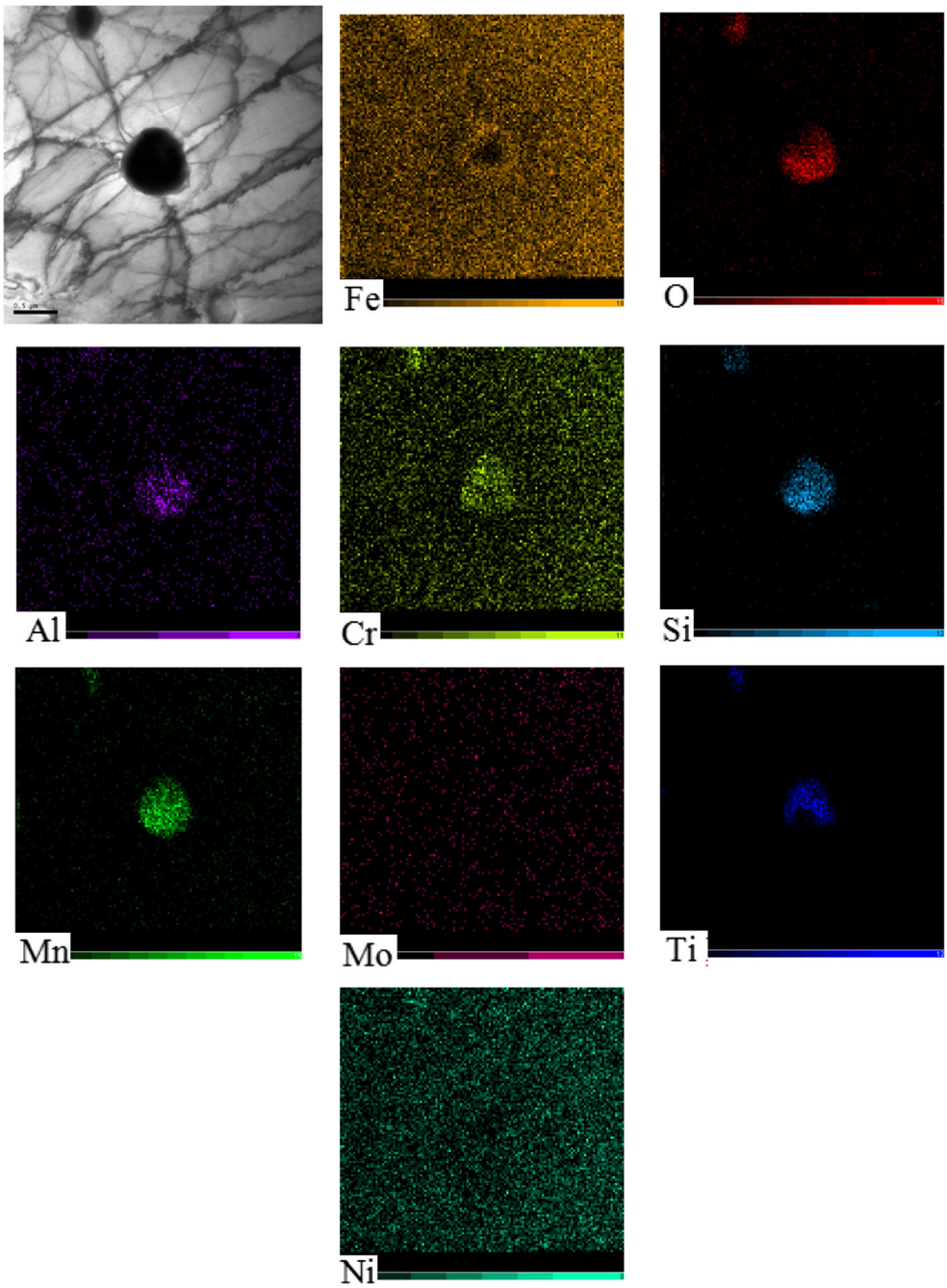

Fig. 14 TEM mapping analysis taken from metal joined with %100 CO_2 shielding gas

Although impact toughness in materials having FCC structure does not change a lot based on test temperature, the existence of δ-ferrite in certain amounts in weld metal causes to decrease toughness value at low test temperatures. The impact toughness values obtained from samples with higher δ-ferrite content in the weld metal are also higher. In fact, although the impact toughness values should be higher in samples with higher austenite phase, the increase in the amount of inclusions created in the microstructure of the weld metal in line with the increased amount of CO_2 cause the decrease of the impact toughness values of the welded materials, despite the high amount of austenite in the weld metal. This shows that the inclusions formed in the weld metal are more effective than the amount of austenite and δ-ferrite phase. It has been reported that increased amount of CO_2 in the shielding gas reduces δ-ferrite amount of the weld metal and leads to the formation of oxides such as Si_2O and MnO in the weld metal [12–14, 16, 17].

Figure 10 shows the SEM image taken from the inclusion on the fracture surface seen after the impact test applied to the weld metal of the AISI 316 L austenitic stainless steel material welded using 100 % CO_2 shielding gas, in order to better see the

inclusions. As shown in the figure, the pits where the inclusions are located are deeper, and there are gaps right next to the inclusions. There are cleavage fracture zones with a flat appearance on the morphology of the inclusion's fracture surface. The structures located on the inclusion form draws attention.

SEM image and the point EDS analysis of the inclusion formed in the weld metal of the materials welded using 100 % CO_2 shielding gas are shown in Fig. 11. O, Si, Ti, Al, and Mn peaks are observed in the EDS analysis of the inclusion. And the ratio of Cr and Ni elements is significantly lower than normal. EDS analysis show that inclusions are formed of different oxides, in other words of multiple oxides. Since Si and Mn in the weld metal do not behave as deoxidant at above 1800 °C, they precipitate as microparticles [17]. The heat input that was increased due to use of 100 % CO_2 shielding gas increases the diffusion of oxygen in the weld pool [32]. It is understood that they combine with elements having high affinity to oxygen such as Si, Mn, Ti, and Al and create multiple oxide forms. As far as it can be understood from the EDS analysis, the oxygen causes the formation of inclusion in the weld metal because of the increased heat in the weld pool, and the ones formed on the surface of the weld pool are added to slag created due to melting of the flux of the additional metal. Inclusions are probably composed of FeO, CrO, Si_2O, TiO_2, MnO, and Al_2O_3, and their sizes vary between 1 to 8 μm.

3.7 TEM-EDS analyses

The mechanical, microstructural, and characterization tests performed in order to prove the effect of shielding gas during welding of AISI 316 L stainless steel material in the applied the experimental studies showed the effect of CO_2 gas on the weld metal. However, TEM/EDS analyses were performed in order to be able to perform more detailed studies of the inclusions formed in the weld metal. Much smaller size inclusions were found in the microstructure in TEM analysis, and characterization of these inclusions was carried out. Figure 12 shows the TEM image of inclusions in the weld metal and the EDS analysis of the inclusion. The chemical composition of an inclusion as revealed by TEM-EDS (Fig. 12b) is as follows: O:31.4 %, Al:1.7, Si:10.9, Ti:21.9, Cr:9.6, Mn:21.6, Fe:2.8. TEM/EDS analysis result shows that multiple oxides are formed in the weld metal depending on the increased amount of CO_2 in the shielding gas mentioned previously and confirms the information obtained in SEM/EDS studies.

And Fig. 13 shows the linear analysis results of the inclusions in the weld metal microstructures. Elements in the form of oxide came to the fore in linear analysis results. These are presented in Fig. 13b as O, Si, Ti, Al, Mn, and Cr concentration graphs.

TEM-EDS analysis result shows that multiple oxides are formed in the weld metal depending on the increased amount of CO_2 in the weld metal mentioned previously and confirms the information obtained in SEM-EDS studies. Also, EDS elemental mapping of the inclusions occurred in the various zones are taken and the distribution of elements in the structure of the multiple oxide form was studied, in order to better characterize the multiple oxide formation (Fig. 14). Cr, Si, Ti, Al, Mn, and O elements were identified in the mapping process. However, Al, Ti, and O elements decrease in some parts of the oxide inclusion. The elements in the structure are not uniform. TEM-mapping analysis clearly confirms that the inclusions are formed of Al_2O_3, CrO, SiO_2, MnO, TiO_2 oxides.

4 Conclusions

- Austenite area expands and the amount of δ-ferrite phase decreases in the microstructure, depending on the ratio of CO_2 in the shielding gas.
- Low amounts of CO_2 shielding gas cases the dendritic branches of δ-ferrite form in a linear elongation shape, whereas with the increase in the amount of CO_2, breaks, openings, and splits are observed in dendrite branches with the welding performed in especially the Ar-50 % CO_2 and 100 % CO_2.
- The increase in the amount of CO_2 in the shielding gas during the welding process forms spherical inclusions in the weld metal by creating various reactions. It was determined that the amount of CO_2 in the shielding gas causes an increase in the number of inclusions in the weld metal.
- Both SEM/EDS and TEM/EDS analysis values reveal that inclusions contain oxygen. It is understood that they combine with elements having high affinity to oxygen such as Si, Mn, Ti, and Al, and create multiple oxide forms. It is suggested that these oxides are complex oxides and consist of Si_2O, TiO_2, MnO, and Al_2O_3.
- A decrease in Charpy impact toughness values was observed as the amount of CO_2 in the shielding gas increases. Impact toughness values are adversely affected by amount and size of inclusions within weld metal. In addition, Charpy impact test temperature also affects the fracture toughness energies, and lower toughness values are obtained at low temperatures.

Acknowledgments This work was carried out as a part of Project (grant no: Commission for Scientific Research Project (BAPK) 2011-50-02-018) supported by the Sakarya University. Both authors would like to thank the University, and M. Tümer would like to thank the Gedik Welding Inc.

References

1. Lippold JC, Kotecki DJ (2005) Welding metallurgy and weldability of stainless steels. Wiley, NJ

2. Jang AY, Lee DJ, Lee SH, Shim JH, Kang SW, Lee HW (2011) Effect of Cr/Ni equivalent ratio on ductility-dip cracking in AISI 316L weld metals. Mater Des 32:371–376
3. Kianersi D, Mostafaei A, Amadeh AA (2014) Resistance spot welding joints of AISI 316L austenitic stainless steel sheets: phase transformations, mechanical properties and microstructure characterizations. Mater Des 61:251–263
4. Kim YH, Lee DJ, Byun JC, Jung KH, Kim JI, Lee HJ, Shin YT, Kim SH, Lee HW (2011) The effect of sigma phases formation depending on Cr/Ni equivalent ratio in AISI 316L weldments. Mater Des 32:330–336
5. Katherasan D, Srivastava S, Sathiya P (2013) Process parameter optimization of AISI 316L(N) weld joints produced using flux-cored arc welding process. Trans Indian Inst Met 66(2):123–132
6. Gençkan D, Saraçoğlu E (2009) Özlü Tel Kaynak Teknolojisi. Mühendis ve Makine 50(599):74–77
7. Engindeniz E (2010) MAG Welding of High Strength Special-Purpose Structural Steel With Flux Cored Wires. 63rd Annual Assembly & International Conference of the International Institute of Welding. 2010, 18–13
8. Katherasan D, Sathiya P, Raja A (2013) Shielding gas effects on flux cored arc welding of AISI 316L (N) austenitic stainless steel joints. Mater Des 45:43–51
9. Aloraier A, İbrahim R, Thomson P (2006) FCAW process to avoid the use of post weld heat treatment. Int J Press Vessel Pip 83:394–398
10. Tümer M, Yılmaz R (2011) The Effects of Welding Parameters and Gases Composition on Microstructure and Penetration of Stainless Steels. International Congress on Advances in Welding Science and Technology for Construction, Energy and Transportation Systems. 24-25 October, AWST-11/103, Antalya
11. Yılmaz R, Tümer M (2010) The effect of shielding gases on the microstructure and toughness of stainless steels weldments by FCAW. 63rd Annual Assembly& International Conference of the International Institute of Welding, pp. 847–852, Istanbul
12. Yılmaz R, Tumer M (2013) Microstructural studies and impact toughness of dissimilar weldments between AISI 316 L and AH36 steels by FCAW. Int J Adv Manuf Technol 67:1433–1447
13. Liao MT, Chen PY (1998) The effect of shielding-gas compositions on the microstructure and mechanical properties of stainless steel weldments. Mater Chem Phys 55:145–151
14. Liao MT, Chen WJ (1999) A comparison of gas metal arc welding with flux-cored wires and solid wires using shielding gas. Int J Adv Manuf Technol 15:49–53
15. Sathiya P, Aravindan S, Soundararajan R, Noorul HA (2009) Effect of shielding gases on mechanical and metallurgical properties of duplex stainless-steel welds. J Mater Sci 44:114–121
16. Arivazhagan B, Sundaresan S, Kamaraj M (2009) A study on influence of shielding gas composition on toughness of flux cored arc weld of modified 9Cr–1Mo (P91) steel. J Mater Process Technol 209:5245–5253
17. Mukhopadhyay S, Pal TK (2006) Effect of shielding gas mixture on gas metal arc welding of HSLA steel using solid and flux-cored wires. Int J Adv Manuf Technol 29:262–268
18. Sathiya P, Mishra MK, Shanmugarajan B (2012) Effect of shielding gases on microstructure and mechanical properties of super austenitic stainless steel by hybrid welding. Mater Des 33:203–212
19. Hu ML, Yang TC, Wu HC, Chen C (2005) Fusion zone purification of metal containing oxide inclusions via laser welding. J Mater Sci 40:4125–4127
20. Cleiton CS, Hélio CM, Hosiberto BS, Jesualdo PF (2009) Microstructure, hardness and petroleum corrosion evaluation of 316L/AWS E309MoL-16 weld metal. Mater Charact 60:346–352
21. Vijayanand VD, Laha K, Parameswaran P, Ganesan V, Mathew MD (2014) Microstructural evolution during creep of 316LN stainless steel multi-pass weld joints. Mater Sci Eng A 607:138–144
22. Larry J, Lawrence B (2009) Welding Skills, Processes and Practices for Entry-Level Welders: Book 2, 1st Edition Delmar Cengage Learning, ISBN-10: 1435427904, ISBN-13: 978-1435427907
23. Sato M, Suda K, Nagasaki H (1997) How to weld using flux-cored wires. Weld Int 11(4):264–272
24. Kah P, Martikainen J (2013) Influence of shielding gases in the welding of metals. Int J Adv Manuf Technol 64:1411–1421
25. Slania J (2002) Investigations into the effect of the gas-mixture ionization potential, linear energy of welding, and the conditions for heat extraction on the content of ferrite in austenitic-steel welds. Weld Int 16(10):761–766
26. Norrish J (2006) Advanced Welding Processes. Woodhead Publishing in Materials 82-25
27. Valiente Bermejo MA, Karlsson L, Svensson LE, Hurtig K, Rasmuson H, Frodigh M, Bengtsson P (2015) Effect of shielding gas on welding performance and properties of duplex and superduplex stainless steel welds. Weld World 59: 239–249
28. Kaçar R, Baylan O (2004) An investigation of microstructure/property relationships in dissimilar welds between martensitic and austenitic stainless steels. Mater Des 25:317–329
29. Sun Z, Kuo M, Annergen I, Pan D (2003) Effect of dual torch technique on duplex stainless steel welds. Mater Sci Eng A 356: 274–282
30. Wang S, Ma Q, Li Y (2011) Characterization of microstructure, mechanical properties and corrosion resistance of dissimilar welded joint between 2205 duplex stainless steel and 16MnR. Mater Des 32:831–837
31. Dieter GE (1988) Mechanical metallurgy. McGraw-Hill, London, p 476
32. Lu S, Fuji H, Nogi K (2005) Effects of CO_2 shielding gas additions and welding speed on GTA weld shape. J Mater Sci 40:2481–2485